Article:
Zhang, W, Wang, F, Wang, Y et al. (5 more authors) (2016) pH and near-infrared light dual-stimuli responsive drug delivery using DNA-conjugated gold nanorods for effective treatment of multidrug resistant cancer cells. Journal of Controlled Release, 232. pp. 9-19. ISSN 0168-3659

https://doi.org/10.1016/j.jconrel.2016.04.001

pH and near-infrared light dual-stimuli responsive drug delivery using DNA-conjugated gold nanorods for effective treatment of multidrug resistant cancer cells

Wenjun Zhang, Feihu Wang, Yun Wang, Jining Wang, Yanna Yu, Shengrong Guo*, Rongjun Chen*, Dejian Zhou*

ABSTRACT

A thiolated pH-responsive DNA conjugated gold nanorod (GNR) was developed as a multifunctional nanocarrier for targeted, pH-and near infrared (NIR) radiation dual-stimuli triggered drug delivery. It was further passivated by a thiolated poly(ethylene glycol)-biotin to improve its cancer targeting ability by specific binding to cancer cell over-expressed biotin receptors. Doxorubicin (DOX), a widely used clinical anticancer drug, was conveniently loaded into nanocarrier by intercalating inside the double-stranded pH-responsive DNAs on the GNR surface to complete the construction of the multifunctional nanomedicine. The nanomedicine can rapidly and effectively release its DOX payload triggered by an acidic pH environment (pH ~5) and/or applying an 808 nm NIR laser radiation. Compared to free DOX, the biotin-modified nanomedicine displayed greatly increased cell uptake and significantly reduced drug efflux by model multidrug resistant (MDR) breast cancer cellines (MCF-7/ADR). The application of NIR radiation further increased the DOX release and facilitated its nuclear accumulation. As a result, this new DNA-GNR based multifunctional nanomedicine exerted greatly increased potency (~67 fold) against the MDR cancer cells over free DOX.

Keywords: I-motif DNA, Gold nanorod, Dual-responsive drug delivery, Near infrared radiation, Multidrug resistance, Cancer

1. Introduction

Breast cancer is the most common cancer in women, with more than 1.38 million new cases diagnosed resulting in approximately 458,400 deaths every year [1]. Although current treatments such as surgical intervention, radio therapy, and chemotherapy can provide significant benefits, they also cause collateral and adverse side-effects to patients [2]. These are mostly caused by the inherent invasive nature of surgical treatment and/or lacking of specific targeting ability of small-molecule based therapeutic treatments, leading to cytotoxic drugs randomly distributed inside the body, causing side-effects and toxicity to patients. This limits the dose regime, allowing tumor to gain resistance, and more severely, multidrug resistance (MDR) [3,4]. MDR is a leading cause of cancer chemotherapy failure [5,6], mainly caused by cancer cell surface over-expressed efflux transporters which can effectively efflux out therapeutic drugs, preventing drug accumulation and compromising therapeutic efficacy [7-12]. These problems can potentially be overcomed by nanoscale drugs (nanomedicines) which have completely different cell uptake mechanisms and intracellular pathways from free drugs: endocytosis versus non-specific diffusion. Nanomedicine can deliver the therapeutic drugs deeply into the target cell interiors, making cell surface efflux transporters much less effective, and hence

bypassing a major MDR mechanism [13-16]. Moreover, it can also exploit the unique pathological characteristics of cancer tumors, such as the enhanced permeation and retention (EPR) effect and over-expressed specific receptors to achieve passive [17,18] and active [19-22] targeted drug delivery and therapy, thereby increasing therapeutic efficacy and reducing side-effects. A number of different targeting ligands, such as antibodies [23-25], aptamers [26,27], folate [28] and RGD peptides [29,30] which can recognize specific cancer cell surface over-expressed receptors have been employed for successful cancer targeting.

Over the past 10 years, functional inorganic nanomaterials have been demonstrated as powerful probes in broad biodiagnostic and therapeutic applications. In this regard, gold nanorods (GNRs) have shown great promises in cancer imaging, drug/gene delivery and photothermal therapy, due to excellent biocompatibility, low-/non-cytotoxicity, and unique size- and shaped- dependent physical/chemical properties [31]. Particularly, GNRs display two distinct absorption bands, a weaker band at shorter wavelengths and a stronger band at longer wavelengths, corresponding to transverse and longitudinal surface plasmon resonance (LSPR) absorption bands, respectively. Moreover, the LSPR band absorption can be tuned to cover from visible to near-infrared (NIR) and to even infrared regions of spectrum by changing aspect ratio [32,33]. As a result, the strong GNR LSPR absorption band can be tuned to overlap with the NIR transmission window of biological tissues, where NIR radiations which have deep tissue penetration can be effectively absorbed by GNRs and converted into localized heat for effective photothermal therapy [34-40].

An effective anticancer nanomedicine should not only display high cell uptake, but also be able to exploit specific environmental stimuli to achieve effective release of drug payload at target sites. In this regard, pH is an attractive environmental stimulus for cancer targeting because the tumor center (*ca.* pH 6.5-6.8) as well as the intracellular endosomes/lysosomes (*ca.* pH 4.3-6.8) are known to be more acidic than healthy tissues [41,42]. We have previously shown that a single-stranded DNA containing 4-stratches of cytosine rich sequences can be reversibly switched between a C-quadruplex (also known as i-motif) [43-45] and single-stranded (or double-stranded upon hybridization to a complementary strand) structure by cycling the environmental pH between 5 and 7.4 [46,47]. The critical pH for i-motif structure formation is ~pH 6.4, making it well-suited for cancer targeting via the acidic local environment [48-53]. By conjugating multiple i-motif DNA strands onto a gold nanoparticle (GNP) *via* gold-thiol self-assembly, we have successfully developed an i-motif DNA-GNP based drug nanocarrier that can exploit the intracellular endo-/lyso-somal acidic environment to achieve efficient, pH-triggered release of intercalated doxorubicin (DOX) inside cancer cells, leading to high cytotoxicity [54]. Moreover, we have further improved the stability and resistance of the DNA-GNP conjugate against nuclease degradation *via* a new PEGylation strategy [55]. The PEGylated DNA-GNP still retained attractive properties such as high cell uptake, low/non-toxicity, high stability in biological buffers and excellent resistance to nuclease degradation, making it an attractive universal nanocarrier for intracellular delivery of DNA binding agents. However, just as other DNA-GNP system, the universally high cell uptake property made it challenging to be able to target specific cancer cells.

Herein, we report the development of a targeted, dual-stimuli-responsive nanomedicine built upon a biotin-PEG passivated i-motif DNA-GNR conjugate, Biotin-PEG-GNR-DNA/DOX (BPGDD) (Fig. 1). The clinical anticancer drug, doxorubicin (DOX), is stably intercalated within a double-stranded i-motif DNA structure

(abbreviated as dsM1/MC2, where M1 is the thiolated i-motif strand and MC2 is the complementary strand with 2 purposely introduced mismatches to tune the duplex stability) under normal physiological pH [54,55]. Upon exposure to weak acidic environment, the M1 strand forms a stable i-motif structure, dehybridizing the MC2 strand and triggering the release of intercalated DOX. Moreover, unlike previous DNA-GNP designs where GNP mostly acts as a stable nanoscale scaffold, the GNR here also efficiently absorbs and converts NIR-radiation into localized photothermal heating to facilitate NIR-light triggered drug release, presumably *via* heat induced dsM1/MC1 dehybridization. The nanocarrier was further passivated by a thiolated poly(ethylene glycol) biotin (PEG-biotin) to increase stability, prolong blood half-life and reduce toxicity and immunogenicity. The incorporation of biotin also allows the carrier to bind specifically to cancer cell over-expressed biotin receptors for specific cancer cell targeting. BPGDD complexes are characterized and their pH- and NIR radiation dependent DOX release properties are evaluated. Their cell uptake and efflux properties as well as cytotoxicities are evaluated using both drug-sensitive and MDR human breast adenocarcinoma cell lines (MCF-7 and MCF-7/ADR). We show this GNR based multifunctional BPGDD nanomedicine can provide effective, targeted treatment of MDR MCF-7/ADR cancer cells.

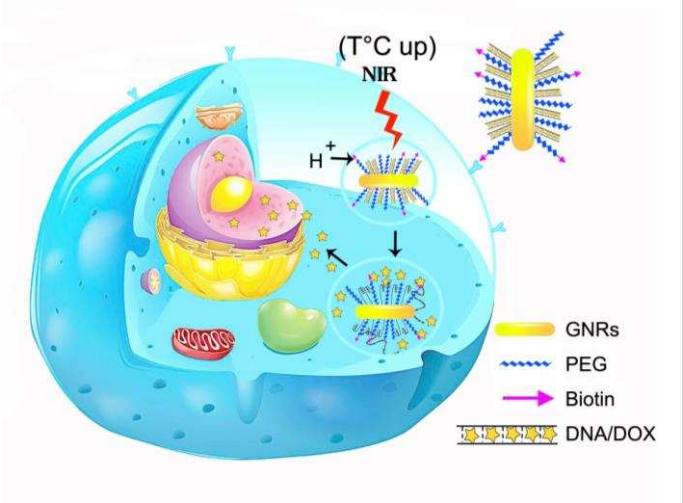

Fig. 1. BPGDD is effectively taken up by cancer cell via binding to its over-expressed biotin receptors and entry into intracellular endosomes. The gradual acidification of the intracellular compartments following the natural endosomal maturation/trafficking pathways lead to i-motif formation and trigger DOX release. Alternatively, DOX release can also be triggered by application of a NIR radiation to locally heats up the GNR carrier.

2. Materials and methods

2.1. Materials

Mercaptoethylamine, dimethyl sulfoxide (DMSO), cetyltrimethylammonium bromide (CTAB), 7-Bromo-3-hydroxy-2-naphthoic acid (7-BrHNA), sodium borohydride (NaBH4), silver nitrate (AgNO3), L-ascorbic acid (L-

AA), 3-(4,5-dimethylthiazol-2-yl)-2,5-diphenyltetrazolium bromide (MTT), bisBenzimide H 33342 trihydrochloride (Hochest 33342) and trypan blue were purchased from Sigma Co., Ltd. (USA). mPEG (Mw = ~2000 Da), 3-mercaptopropionic acid (MPA), 1-ethyl-3-(3-dimethylaminopropyl)-carbodiimide hydrochloride (EDC·HCl), 1-hydroxy benzotriazole (HOBT), 4-dimethylamino pyridine (DMAP), 2-(N-Morpholino) ethanesulfonic acid (MES), Tris (2-carboxyethyl) phosphine hydrochloride (TCEP·HCl), 1-dodecanethiol (DDT) and 11-mercaptoundecanoic acid (MUDA) were purchased from Aladdin Industrial Co., Ltd. (China). LysoTracker Green was purchased from Invitrogen Molecular Probes (USA). Chloroauric acid ($HAuCl_4 \cdot 3H_2O$), hydrochloric acid, nitric acid and toluene were purchased from Sinopharm Chemical Reagent Co., Ltd. (China). Methanol, acetone, isopropyl alcohol and sodium chloride were purchased from Shanghai Ling Feng Chemical Reagent Co., Ltd. (China). Biotin-PEG-NHS (Mw = ~2000 Da) was purchased from Jenkem Technology Co., Ltd. (China). M1, MC2 (see Table 1 for sequences) were purchased from SBS Genetech Co., Ltd. (China). Doxorubicin (DOX) was purchased from Beijing Huafeng Lianbo Technology Co., Ltd.

The human breast cancer cell lines (MCF-7 and MCF-7/ADR) were obtained from School of Pharmacy, Shanghai Jiao Tong University. The Roswell Park Memorial Institute 1640 (RPMI-1640), penicillin–streptomycin, fetal bovine serum (FBS), 0.25%(w/v) trypsin–0.03% (w/v) EDTA solution and phosphate buffer solution (PBS) were purchased from Gibco BRL (USA). Water was purified by distillation, deionization, and reverse osmosis (Milli-Q plus). All chemicals were analytical grade and were used as received without further purification.

2.2. Synthesis of GNRs

GNRs with a peak absorption wavelength of 808 nm were synthesized using a seed-mediated growth method [56,57]. Briefly, a seed solution for GNRs was prepared by mixing 5 mL of 0.5 mM $HAuCl_4$ with 5 mL of 0.2 M CTAB solution, and 0.6 mL of 0.01 mM $NaBH_4$ (fresh ice-cold) was added. After 2 min of stirring (1200 rpm), the seed solution was aged at 30℃ for 2 h before use. The growth solution was prepared by dissolving 1.0800 g of CTAB and 0.0612 g of 7-BrNHA [58] in 30 mL of warm water (30℃) in a 100-mL flask. Afterwards, 0.96 mL of 4 mM $AgNO_3$ solution was added and kept standing for 15 min, followed by the addition of 30 mL of 1 mM $HAuCl_4$ solution and 100 μL HCl under slow stirring (400 rpm) for 15 min. Subsequently, 300 μL of freshly prepared L-ascorbic acid (0.064 M) was added to the growth solution. After a vigorous stirring for 60 s, the seed solution was injected into the growth solution. The resulting mixture was stirred for 30 s and left standing overnight for GNRs growth. The reaction products were isolated by centrifugation at 10000 rpm for 20 min followed by removal of the supernatant. The precipitates were re-dispersed in 1 mL of water.

2.3. Synthesis of 11-mercaptoundecanoic acid (MUDA) capped GNRs

The CTAB surfactants on the GNR surface were replaced through the round-trip phase transfer ligand exchange reported by Wijaya et al [59]. Specifically, 1 mL of 20-50 nM GNRs-CTAB in water was put into

contact with 1 mL of dodecanethiol (DDT). Then 3 mL of acetone was added and the solution was swirled for a few seconds to extract GNRs into DDT, upon which the aqueous phase became clear. Next, GNR-DDT were diluted in 5 mL of toluene to remove excess DDT, centrifuged at 8000 rpm for 15 min, and then re-suspended in 1 mL of toluene by sonication. The GNR-DDT in toluene were then added to 9 mL of 0.01 M mercaptoundecanoic acid (MUDA) in toluene at 70 ℃ and vigorously stirred. Refluxing and stirring continued until visible aggregation was observed (in 15 min), and then the solution was allowed to settle and cool to room temperature. The aggregates were washed twice with 1 mL of toluene via decantation and then once with 1 mL of isopropanol to deprotonate the carboxylic acid. The aggregates spontaneously re-dispersed in 1× tris-borate-EDTA (TBE) buffer.

2.4. Synthesis of HS-PEG

To synthesize HS-PEG (Fig. 3A.), 3-mercaptopropionic acid (MPA) was first activated with EDC to enhance the conjugation efficiency, through reaction with EDC, HOBT and DMAP at the molar ratio MPA: EDC: HOBT: DMAP of 1: 2: 2: 0.2 in 5 mL of DMSO under a N_2 atmosphere for 4 h at room temperature. The activated MPA was then added to 2 mL of 1 mM mPEG2000 in DMSO and the mixture was stirred under N_2 atmosphere for 48 h. Then, the products were dialyzed for 2 days using a dialysis tube (molecular weight cut-off = 1000 Da) to remove unreacted materials. The resulting HS-PEG was obtained after freeze drying and its chemical structure was confirmed by the ^{1}H-NMR spectra recorded on a Varian Mercury Plus-400 NMR spectrometer (Varian, USA).

2.5. Synthesis of HS-PEG-Biotin

The synthesis route of HS-PEG-Biotin was shown in Fig. 3A. Briefly, 200 mg Biotin-PEG2000-NHS and 129.6 mg mercaptoethylamine (at the molar ratio of 1:20) were dissolved in 2 mL of DMSO and stirred under N_2 atmosphere at room temperature. After 48 h, products were dialyzed for 2 days using a dialysis tube (molecular weight cut-off = 1000 Da) to remove unreacted materials. The resulting HS-PEG-Biotin was obtained after freeze drying and its chemical structure was confirmed by ^{1}H-NMR.

2.6. Preparation of HS-DNA/DOX

To synthesize HS-DNA/DOX, M1 was mixed with MC2 at the molar ratio of 1:1 in 500 μL of MES buffer (50 mM MES, 150 mM NaCl, pH 7.4) and hybridized for 4 h at 37 °C to form dsDNA, which were then titrated into DOX in MES buffer [53]. Different molar ratios of DNA base pair to DOX were used to determine the optimized DOX loading condition. The change of DOX fluorescence intensity was monitored using a F-7000 fluorescence spectrophotometer (Hitachi, Japan) to evaluate DOX-dsDNA binding.

2.7. Synthesis of Biotin-PEG-GNR-DNA/DOX (BPGDD) nanocarrier

GNR-MUDA and HS-PEG were mixed at the molar ratio of 1:50,000 and stirred for 48 h under N_2 atmosphere.The resulting GNR-PEG was centrifuged at 10,000 rpm for 20 min and then washed twice with water to remove any residual reactants. The GNR-PEG precipitates were re-dispersed in 1 mL of water. Then, HS-DNA/DOX and HS-PEG-Biotin (at a molar ratio of 10:1) were dissolved in 4 mL of water, followed by addition of 1 mL of GNR-PEG and stirring for 48 h under a N_2 atmosphere. The resulting Biotin-PEG-GNR-DNA was purified by centrifugation, washed and re-dispersed in 1 mL of water. Finally, Biotin-PEG-GNR-DNA and DOX were incubated for 4 h at the molar ratio of 1:40,000. The resulting Biotin-PEG-GNR-DNA/DOX (BPGDD) nanocarrier was obtained after centrifugation and re-dispersed in 1 mL of water.

Absorbance of the GNRs was measured using a U-2910 UV–Vis–NIR spectrophotometer (Hitachi, Japan). Zeta potential was measured using a Zetasizer NanoZS/ZEN3600 (Malvern Instruments, Herrenberg, Germany). Morphology and size were measured using a JEOL JEM-2100F transmission electron microscope (TEM) (Japan).

2.8. Dual-stimuli triggered DOX release

2.8.1.pH-responsive DOX release

200 μL of BPGDD complexes was diluted with a PBS buffer at specific pH ranging from 5.0 to 7.4 to a final DOX concentration at 2 μM in a 96-well plate. At various time intervals, the concentrations of DOX released from BPGDD complexes were measured using a F-7000 fluorescence spectrophotometer (Hitachi, Japan).

2.8.2. NIR-triggered DOX release

200 μL of BPGDD complexes in PBS buffer (pH 5.0) was added to each well of a 96-well plate and irradiated with the NIR laser light (LE-LS-808-2000 T-FCA, LEO Photonics, China) at 808 nm with a 5 mm diameter spot-size at a power density of 1.0, 2.5, 5, 7.5, 10 w/cm^2 for different periods of time (up to 30 min). The solution temperatures were detected with a HH508 digital thermometer (Omega, Switzerland), and concentrations of DOX released were detected with a fluorescence spectrophotometer as mentioned above.

2.9. Cell culture

The human breast adenocarcinoma cell line MCF-7 and the ADR-resistant breast cell line MCF-7/ADR were cultured in RPMI-1640 medium supplemented with 10% fetal bovine serum (FBS) and 1% penicillin/streptomycin. The cells were trypsinized using trypsin-EDTA and maintained in a humidified atmosphere supplemented with 5% CO_2 at 37 °C.

2.10. Cellular uptake

MCF-7 and MCF-7/ADR cells were seeded into 24-well plates at a density of $1.5x10^5$ cells per well and cultured for 24 h at 37 °C. The cells were then treated with free DOX, GNR-DNA/DOX (GDD) and BPGDD at 0.25 μM DOX concentration for various durations of time. Untreated cells served as a negative control. Then cells were washed three times with cold PBS and fixed with 4% paraformaldehyde solution. The cellular uptake was quantitatively determined by a BD LSRFortessa flow cytometry (Becton Dickinson, USA). The mean fluorescence signal for 10,000 cells was recorded and all experiments were repeated three times.

2.11. Efflux studies

MCF-7/ADR cells were seeded into 24-well plates and cultured for 24 h. The spent medium was removed and the cells were incubated with free DOX, GDD and BPGDD at 2 μM DOX concentration. After for 4h, the cells were washed twice by PBS and then replenished with a fresh complete medium. After incubation for a specific duration of time ranging from 0.5 to 8 h, the cells were washed three times with cold PBS and fixed with 4% paraformaldehyde solution. The cellular efflux was quantitatively determined by flow cytometry.

2.12 Cellular accumulation under NIR irradiation

The photothermal effect was evaluated by following previously established procedures. MCF-7/ADR cells were incubated with BPGDD at 2 μM DOX concentration for 4 h, washed three times with cold PBS, and then replenished with a fresh complete medium. Half of cells were irradiated at 808 nm with a 5 mm diameter spot-size at 5 W/cm^2 for 10 or 30 min and the other half did not undergo laser irradiation. After incubation for an additional 1 or 4 h, the spent medium was removed and cellular apoptosis was quantitated by flow cytometry.

2.13. Co-localization visualized by confocal laser scanning microscope (CLSM)

To observe the intracellular distribution of the nanocarrier, MCF-7/ADR cells were seeded into 12-well glass-bottom plates at a density of 1 x 10^5 cells/well and cultured for 24 h. The cells were then treated with free DOX, GDD and BPGDD at 2 μM DOX concentration. After 2 or 4 h of incubation, the spent medium was aspirated and cells were washed twice with PBS and replenished with a fresh complete medium. Half of cells treated with BPGDDX complexes were irradiated at 808 nm with a 5 mm diameter spot-size at 5 W/cm^2 for 30 min. Afterwards, cells were treated with Hoechst 33342 (6 μg/mL) for 20 min, washed with PBS twice, and fixed with 500 μL of 4% paraformaldehyde for 30 min. The fixed cells were sealed with slides and observed using a confocal laser scanning microscope (TCS SP5, Leica, Germany).

2.14. Evaluation of cytotoxicity

Cytotoxicity of nanocarriers toward cells was assessed using the MTT assay. Firstly, MCF-7 and MCF-

7/ADR cells were seeded into 96-well plates at a density of $4x10^3$ and incubated for 24 h. The cells were then treated with free DOX, GDD and BPGDD at different DOX concentrations. After 48 h of incubation, 200 μL of 0.5 mg/mL MTT in RPMI-1640 was added to each well. After 4 h of incubation, the spent MTT solution was discarded and 200 μl of DMSO was added to dissolve the formazan crystals. The absorbance at 570 nm with a reference wavelength of 630 nm was recorded using a microplate reader (Bio-Rad 680, USA). The inhibition rate of cells = $(A570_{control} - A570_{sample}) / A570_{control} \times 100\%$.

The photothermal effect on cell cytotoxicity was also evaluated, MCF-7/ADR cells were incubated with BPGDD at 2 μM DOX concentration for 4 h, washed twice with PBS and then replenished with the fresh complete medium. The cells were irradiated with an 808nm NIR laser light at 2.5, 5 and 7.5 W/cm^2 for a period of time up to 30 min. After 48 h of incubation, the inhibition rate of cells was evaluated by MTT assay.

2.15. Apoptosis assay

MCF-7/ADR cells were seeded into 12-well plates at a density of $3x10^5$ and cultured for 24 h. The cells were then incubated with DOX, GDD and BPGDD at 2 μM DOX concentration for 4 h, washed three times with PBS, and then replenished by fresh complete medium. Half of the cells treated with BPGDD were then irradiated by an 808 nm laser beam with a 5 mm diameter spot-size at a power density of 5 W/cm^2 for 30 min. After 48 h of incubation, cellular apoptosis was quantitatively determined using Annexin V/PI double staining. The samples were analyzed by the BD LSRFortessa flow cytometry (Becton Dickinson, USA) using the Cell Quest software (Becton Dickinson). The MCF-7/ADR cells without any treatment were used as the negative control for apoptosis. The mean fluorescence signal for 10,000 cells was recorded. BD LSRFortessa flow cytometry (Becton Dickinson, USA)

3. Results and Discussion

3.1. Synthesis and characterization of BPGDD

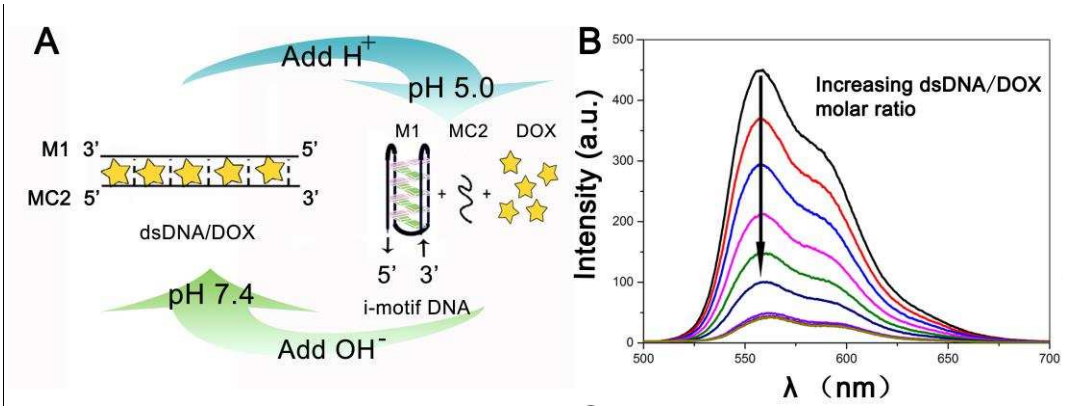

Fig.2. (A) Principle of pH-triggered drug delivery: DOX is intercalated stably within the M1/MC2 duplex at normal physiological pH 7.4, and when pH decreases to ~5.0, M1 forms a four-stranded i-motif structure and

the duplex of dsDNA dissociates and DOX is released. (B) Fluorescence spectra of DOX (20μM) with increasing the dsDNA:DOX molar ratio at pH 7.4.

Table 1

DNA sequence of M1,MC2

DNA code	Sequece(5' 3')
M_1	HS-TTT TTT TTT TCC CTA ACC CTA ACC CTA ACC C
MC_2	GT GTT AGG TTT AGG GTT AGG G

The pH-dependent DOX binding properties of double-stranded (ds) M1/MC2 (see Fig.2A for the principle of pH-triggered drug delivery and Table 1 for the sequences) structure was investigated. As shown in Fig. 2B, a sharp decrease of DOX fluorescence intensity was observed with increasing amounts of dsM1/MC2 being added to free DOX solution at pH 7.4, indicating that DOX was intercalated efficiently to the DNA duplex. Fig. S3 shows the DOX fluorescence quenching saturate at dsM1/MC2:DOX molar ratio of ~0.12, suggesting each dsM1/MC2 can bind up to 8 DOX molecules.

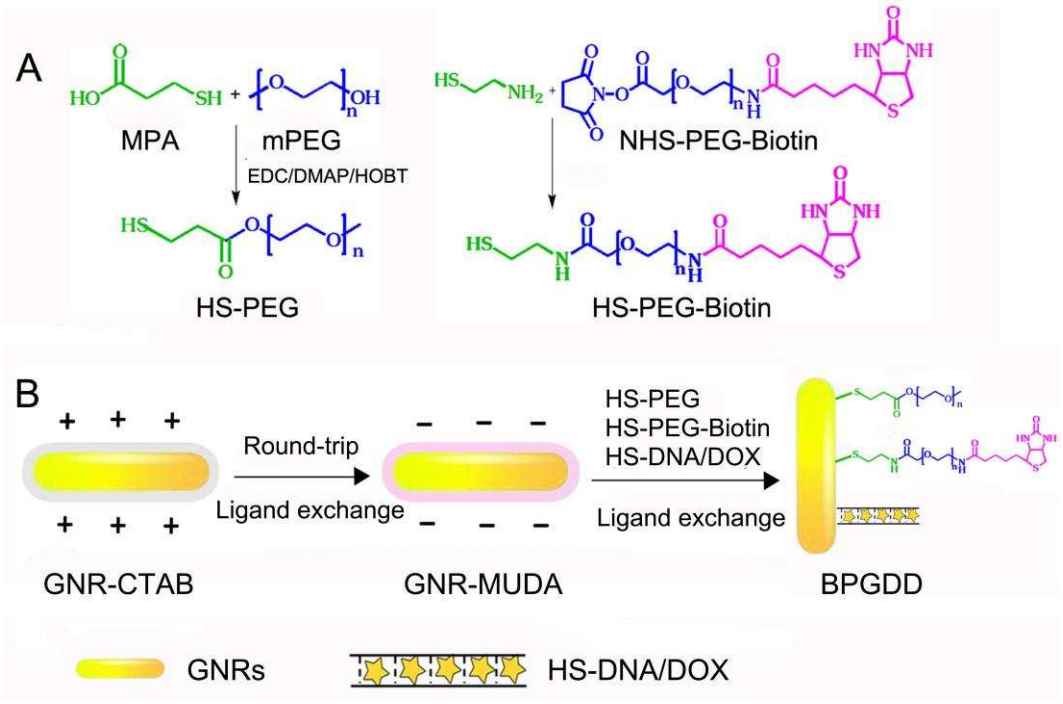

Fig. 3. Schematic route to preparation of (A) HS-PEG and HS-PEG-Biotin, (B) BPGDD multi-functional nanomedicine.

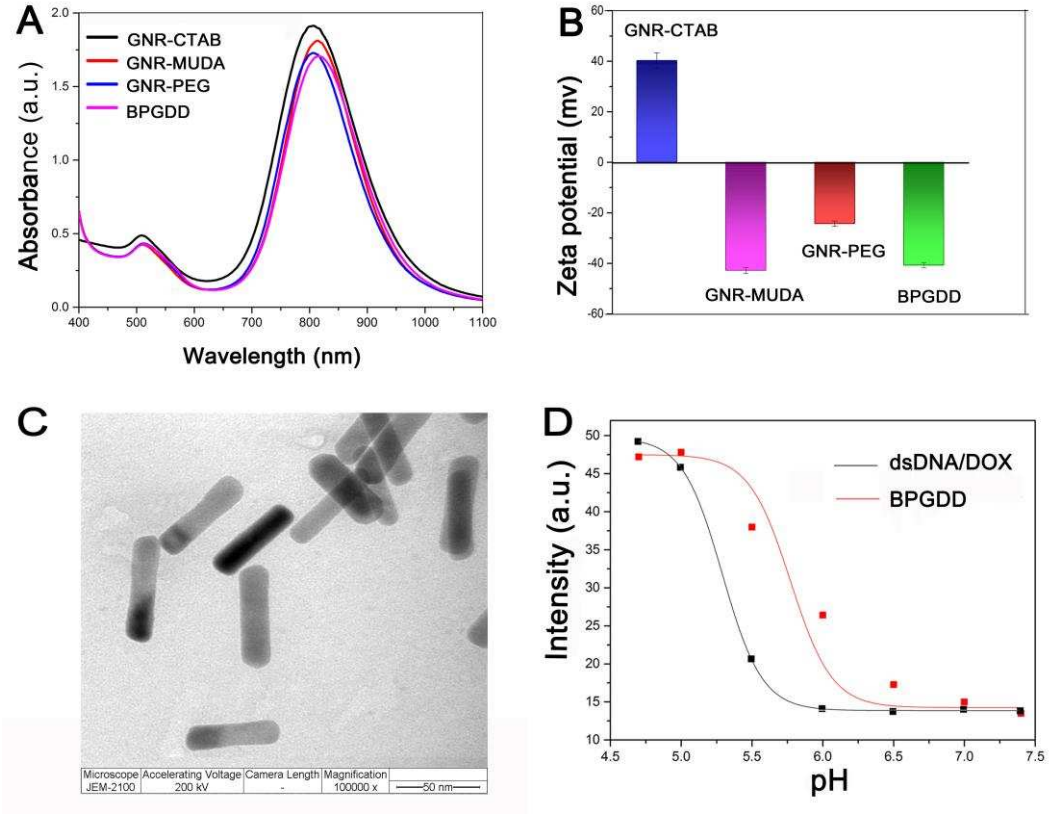

Fig. 4. Characterization of GNR-based systems. (A) UV–Vis–NIR absorption spectra and (B) Zeta potential of of GNR-CTAB, GNR-MUDA, GNR-PEG and BPGDD. (C) A typical TEM image of BPGDD complexes. (D) Dependence of DOX fluorescence intensity as a function of pH for the dsDNA/DOX and BPGDD systems respectively.

Figure 3 show the schematics of our approach to prepare GNR based nanocarriers. Briefly, GNR with an aspect ratio of ~3.5 was prepared by a seed-mediated growth method using cetyltrimethyl ammonium bromide (CTAB) surfactants as reported previously [58]. It was then treated with excess 11-mercapto-undecanoic acid (MUDA) to completely display surface CTAB surfactants to yield GNR-MUDA. This was supported by a complete reversal of zeta potential from +40.2 mV to -42.8 mV (Fig.4B), suggesting the positively-charged CTAB surfactants were completely displaced by the negatively-charged MUDA. GNR-MUDA was then treated with a thiolated-PEG/PEG-biotin (The ^{1}H-NMR spectra are presented in Fig.S1, Fig. S2. The peak at 2.04 ppm is from the proton of SH), displacing some of GNR surface MUDA ligands to form GNR-PEG. This was evidenced by a reduction of negative zeta potential to -24.3 mV because PEG ligand was neutral. The thiolated dsDNA/DOX (DOX loaded dsM1/MC2 structure) was then loaded onto the GNR-PEG-biotin by a simple incubation, leading to the formation of BPGDD multifunctional nanomedicine. The success of the construction was supported by an increase of negative zeta potential to -40.7mv, because the overall DNA-DOX loaded here is negatively charged. The changes of zeta potential in each GNR surface functionalization step matched well to what was expected, indicating these process were successful.

Fig. 4A compares UV-Vis-NIR absorption spectra of different GNR systems: GNR-CTAB, GNR-MUDA,

GNR-PEG and BPGDD. GNR-CTAB showed a TSPR peak at 512 nm and an LSPR peak at 806 nm, suggesting it was an excellent absorption agent for 808 nm NIR radiation. Compared to native GNR, there were negligible changes in UV-Vis-NIR absorption spectra of GNR-MUDA, GNR-PEG and BPGDD, indicating that the surface modifications did not significantly change the unique optical properties of GNRs [60,61]. The TEM image of BPGDD (Fig. 4C) showed typical rod shaped GNRs with an average length of 50 ± 5 nm and diameter of 14 ± 3 nm, giving an aspect ratio of ~3.5 .

Fig. 4D shows the pH-dependent release properties of DOX from dsM1/MC2/DOX and BPGDD systems. The dsDNA/DOX started to release DOX at pH <6.0 with a half-release pH of ~5.4, in good agreement with the literature result [54]. The DOX release from dsM1/MC2/DOX happed very rapidly, saturated DOX release was completed in 30 seconds after pH change. Interestingly, BPGDD system displayed a shifted pH-dependent DOX release character: the onset of DOX release happed at pH ~6.5 with the half-release pH of ~5.8, suggesting it is well-suited for early endosomal release (typical pH 6.0-6.8).

3.2. In vitro pH and NIR laser triggered DOX release

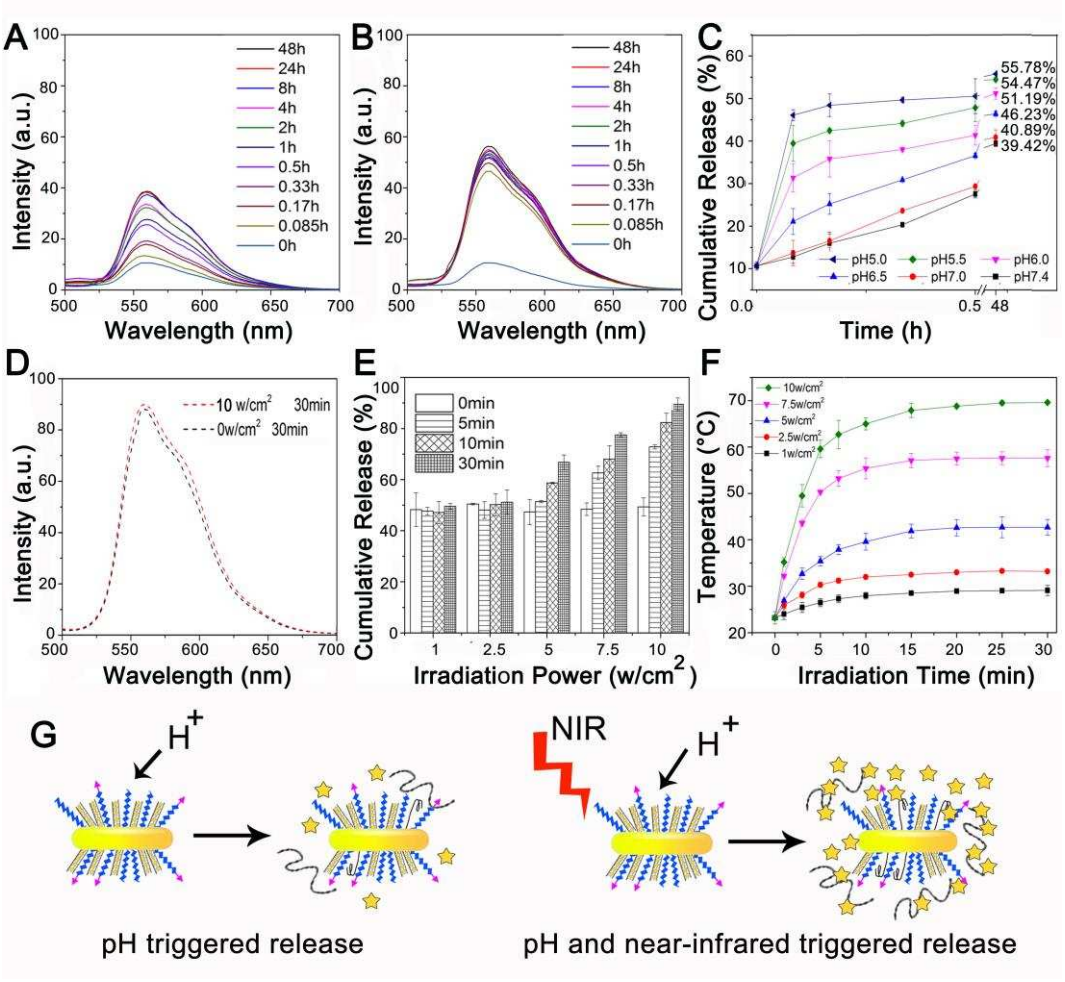

Fig. 5. In vitro DOX release profiles from BPGDD nano-complexes. (A) Fluorescence spectra of the time-dependent release of DOX at pH 7.4. (B) Fluorescence spectra of the time-dependent release of DOX at pH 5.0. (C) Time-dependent accumulative release of DOX at different pH values. (D) Fluorescence spectra of free

DOX before and after NIR irradiation. (E) Time-dependent cumulative DOX release at different NIR radiation power densities (808 nm, 1, 2.5, 5, 7.5 and 10 W/cm^2) at pH 5.0. (F) Time-dependent change of the temperature of BPGDD solution in response to NIR irradiation at different power densities (containing 2 μM DOX and 5.8 μg/mL of GNR). (G) Schematic showing that pH-triggered release alone is less effective than pH- and NIR-light dual-stimuli-triggered DOX release. Data are presented as mean ± SD (n = 3).

To assess pH-dependent release of DOX from BPGDD complexes, the complexes were incubated in PBS buffer at normal physiological pH 7.4 or typical late endosomal pH 5.0. As shown in Fig. 5A, DOX release was low at pH 7.4, where 30 min incubation led to <30% of drug release. Prolonging the incubation time to 48 h led to a modest increase of DOX release to 39.4%, suggesting that DOX was stably intercalated within the dsM1/MC2 DNA structures. Acidification of the buffer to pH 5.0 caused a much higher and faster release, where DOX release was almost complete within 5 min. After 48 h, the cumulative release of DOX at pH 5.0, 5.5, 6.0, 6.5 and 7.0 were found to be 55.8%, 54.5%, 51.2%, 46.2% and 40.9%, respectively. The fluorescence spectra of free DOX before and after exposure to 30 min high power NIR radiation (10 W/cm^2) were almost identical (Fig. 5D), suggesting that NIR irradiation did not affect DOX fluorescence. Fig. 5F revealed that solution temperature was raised rapidly with an increasing NIR radiation power density [62-64], confirming that GNR complexes could convert NIR light energy into heat efficiently and quickly. The increased temperature could dehybridize dsM1/MC2, facilitating DOX release, *e.g.* NIR-radiation could act as a second stimulus to trigger DOX release. This was found to be true, where the combination of NIR radiation and low environmental pH (5.0) achieved accumulative DOX release of 49.6%, 52.3%, 66.8%, 77.5% and 89.5% with a laser power density of 1, 2.5, 5, 7.5 and 10 w/cm^2 over 30 min, respectively (Fig. 5E). These values were significantly higher than that achieved by using pH 5.0 alone (see Fig.5C), confirming that DOX release inside cells can be improved by combined effect of pH decrease and NIR radiation.

3.3. Cellular uptake and efflux

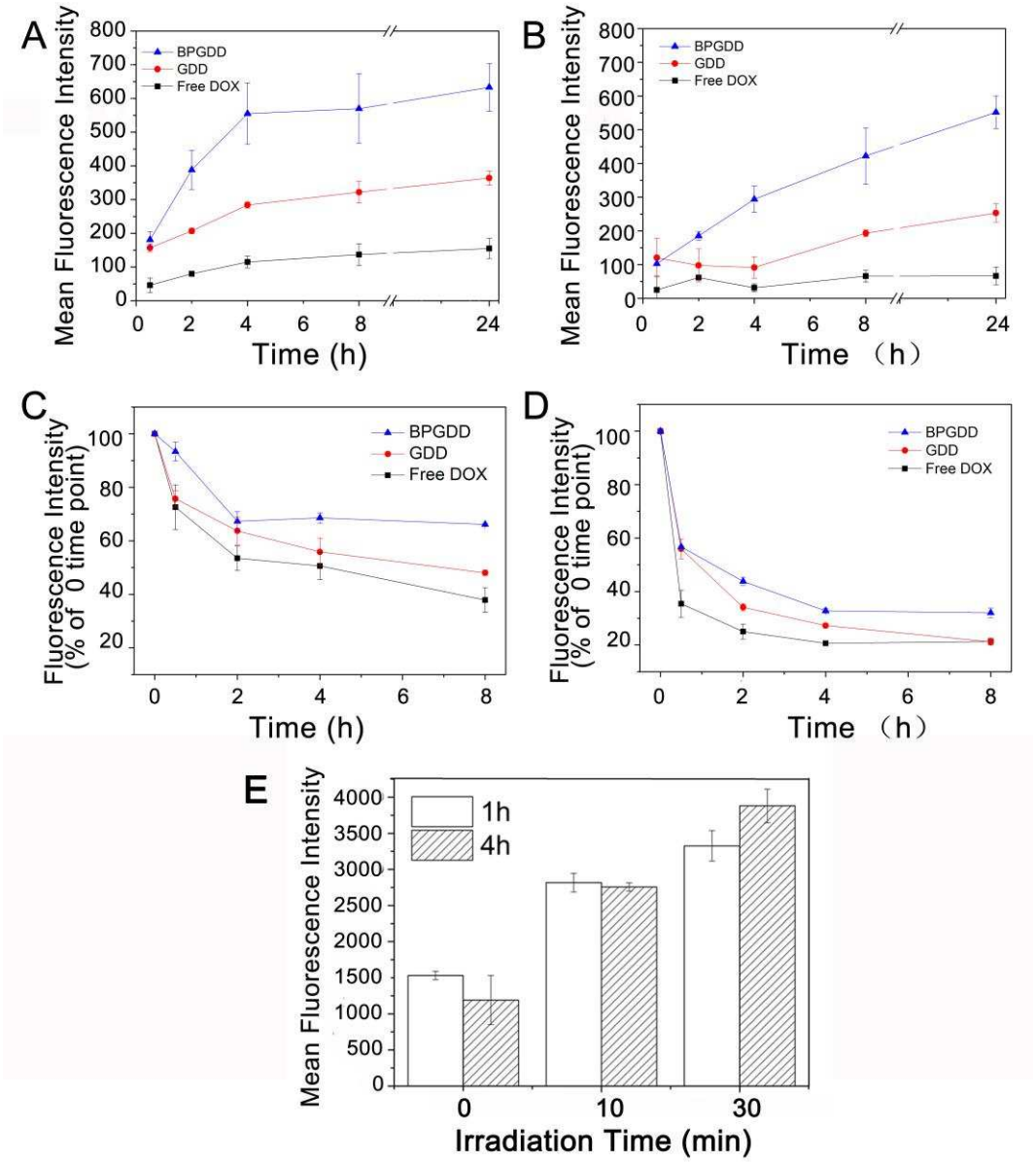

Fig. 6. Time-dependent cellular uptake of DOX by MCF-7 (A) and MCF-7/ADR (B) cells after incubation with free DOX, GNR-DNA/DOX(GDD) and BPGDD (contain 0.25 μM DOX), respectively. Time-dependent efflux of DOX from MCF-7 (C) and MCF-7/ADR (D) cells during the further incubation period (contain 2 μM DOX). (E) Mean DOX fluorescence intensity of MCF-7/ADR cells after incubation with BPGDD (contain 2 μM DOX and GNR 5.82μg/mL) followed by 0, 10 and 30 min of NIR irritation (808 nm, 5 w/cm^2) and 1-4 h further incubation. Data are presented as mean ± SD (n = 3).

The cellular uptake of free DOX, GNR-DNA/DOX (GDD, only dsDNA/DOX loaded GNR) and BPGDD by MCF-7 (Fig. 6A) and MCF-7/ADR cells (Fig. 6B) was examined by flow cytometry. As shown in Fig. 6A, the lowest level of cellular uptake of free DOX by MCF-7 cells was observed and it increased gradually with incubation time. When the cells were treated with GDD, intracellular DOX level was found to be 3.4- or 2.4-fold that of the free DOX treated cells after 0.5 or 24 h incubation, respectively. BPGDD treated cells exhibited

the highest intracellular DOX accumulation, which was 3.9-fold or 4.1-fold that of free DOX treated cells with 0.5 h or 24 h. These results revealed that biotin-modified BPGDD significantly increased DOX accumulation inside cancer cells. Fig.6B revealed that mean DOX fluorescence intensity of free DOX treated MDR MCF-7/ADR cell (66.5 after 24 incubation) was substantially lower than that in the drug sensitive MCF-7 cells (155). Moreover, it did not changed significantly throughout the 24 h treatment period, confirming that the MCF-7/ADR cells can effectively limit the intracellular accumulation of free DOX, possibly due to strong efflux abilities of surface over-expressed efflux transporters (e.g. P-glycoprotein, P-gp). Encouragingly, MCF-7/ADR cells treated with GDD showed a significant increase in intracellular DOX accumulation, being 4.8- and 3.8 fold that of the free DOX controls with 0.5 h or 24 h incubation. More importantly, BPGDD treated cells exhibited the highest level of intracellular DOX fluorescence, being 4.1- and 8.3 fold that of the free DOX control with 0.5 h or 24 h incubation. These results demonstrated that BPGDD could significantly increase the intracellular DOX accumulation in MDR MCF-7/ADR cells, an important factor for high treatment efficacy.

A key cell MDR mechanism is efficient drug efflux by its surface over-expressed efflux pumps (*e.g.* g-glycoproteins), preventing intracellular drug accumulation and compromising treatment efficacy. Here the drug efflux properties were measured by monitoring the retained cellular DOX fluorescence after 4 h treatment with free DOX, GDD or BPGDD during further incubation with fresh medium (Fig.6C and 6D). The normalized the intracellular DOX fluorescence intensities in MCF-7 cells were decreased continuously during the further incubation period, but the downward trends were slower for cells treated by GNR-based nanomedicines than by free DOX. For MDR MCF-7/ADR cells, the intracellular DOX fluorescence decreased much faster than that in MCF-7 cells. This was especially evident for free DOX treatment where only ~38% of original DOX fluorescence was retained after 0.5 h further incubation (versus ~ 72% for MCF-7 cells). These results suggested that the over-expressed efflux transporters on MCF-7/ADR cell surface were efficient at pumping-out intracellular DOX molecules, preventing their built up. The slower DOX efflux rates observed for the GNR-based treatments were presumably due to deeper drug delivery afforded by nanocarriers, making cell-surface efflux transporter less effective.

Moreover, MCF-7/ADR cells after incubation with BPGDD for 4 h followed by NIR radiation at 5 W/cm^2 for 0 (control), 10 and 30 min and further incubated in fresh media at 37 ℃ for another 1 or 4 h were also investigated. Interestingly, cells after treatment with NIR radiation displayed significantly higher intracellular DOX fluorescence intensity (increasing from 1191 to 2757 and 3880 (a.u.) with 10 and 30 min irradiation, respectively), suggesting a substantially increased DOX concentration at the cell interior, presumably due to combined effects of more effective DOX release (as observed in Fig. 5) and significantly compromised DOX efflux ability after NIR laser treatment.

3.4. Confocal imaging BPGDD intracellular delivery to breast cancer

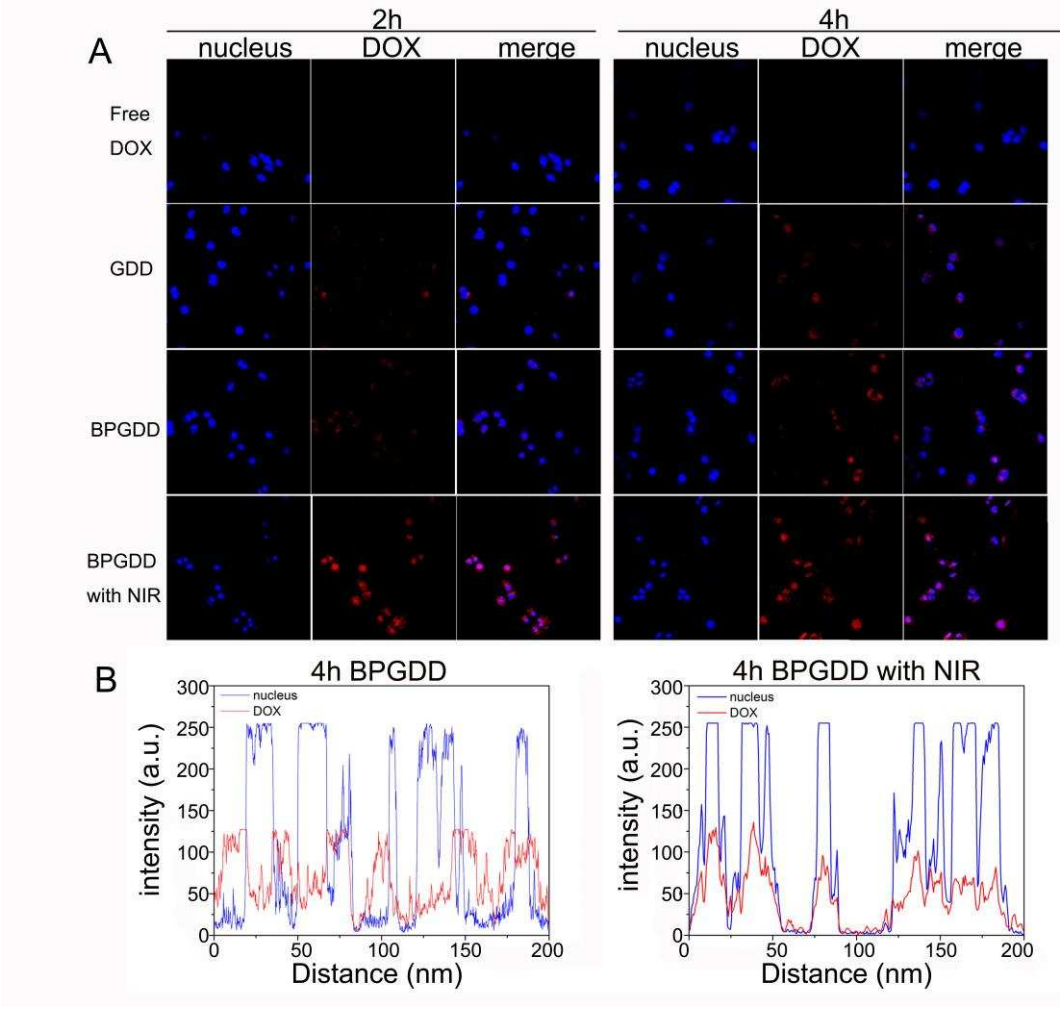

Fig. 7. (A) Confocal fluorescence images showed the intracellular distribution of DOX in MCF-7/ADR cells after treatment with free DOX, GDD, and BPGDD (contain 2 μM DOX and GNR 5.82μg/mL) respectively for 2 or 4 h. (B)The histogram of the nuclei blue-stained with Hoechst 33342 and red-stained with DOX in the MCF-7/ADR cells treated with the BPGDD for 4 h, irradiated with NIR for 30 min or not..

GNR-mediated intracellular DOX distribution was investigated in MCF-7/ADR cells by confocal laser scanning microscopy (CLSM). Fig. 7A showed that when MCF-7/ADR cells were incubated with free DOX (2 μM), only very weak DOX fluorescence was found inside the cells. However, a significantly enhanced intracellular DOX fluorescence was observed for cells treated with GDD and BPGDD, respectively. Moreover, cells treated with BPGDD displayed stronger intracellular DOX fluorescence than those treated by GDD, suggesting biotin-modification on BPGDD significantly increased their uptake by MDR breast cancer cellline. What's more, the DOX fluorescence also increased with the increasing incubation time, presumably due to a gradual uptake and release of DOX payload following a gradually acidified intracellular endo-/lyso-somal environments. Importantly, when cells were treated with NIR irradiation after 4 h uptake of BPGDD, almost all DOX fluorescence was localized in the nucleus, producing almost perfectly overlapped purple-fluorescent spots in merged images. The cross sectional analysis of the above fluorescence image (Fig.7B) further confirmed the perfect red (DOX) and blue (nuclei) fluorescence overlap, suggesting NIR radiation facilitated

the trafficking of DOX into the cell nucleus. This observation may be due to the increased DOX release and enhanced cell membrane permeability induced by GNR based photothermal heating [65].

3.5. Cytotoxictiy evaluation

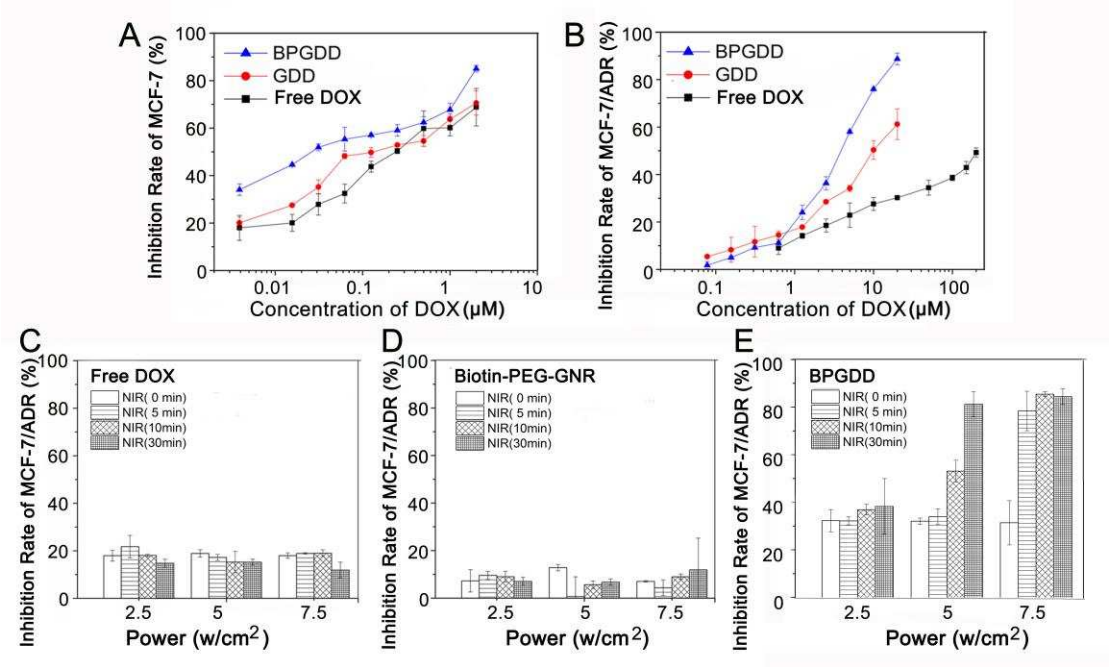

Fig. 8. The inhibition rate of MCF-7 (A) and MCF-7/ADR (B) cells after incubation with free DOX, GDD and BPGDD for 48 h at 37°C as measured by MTT assay. And the inhibition rate of MCF-7/ADR cells after 4 h incubation with free DOX (C), Biotin-PEG-GNR (D), BPGDD (E) (containing 2 μM DOX and GNR 5.82μg/mL), followed by different NIR laser radiation conditions and further 48 h incubation with fresh media. Data are presented as mean ± SD (n = 3).

In vitro cytotoxicity of various GNR-based nanomedicines towards MCF-7 and MCF-7/ADR cells was investigated by MTT assay (see Fig.8) and the IC50 value (the concentration that inhibited cell growth by 50%) was calculated (Table 2). MCF-7/ADR cells displayed a very high IC50 value (251 μM) of free DOX treatment, which was 1192-fold higher than the parent MCF-7 cells (IC50=0.21 μM), consistent to the low DOX accumulation and high efflux ability as observed previously due to over-expressed efflux transporters. Table 2 reveled that GDD and BPGDD showed similar IC50 values (0.17 and 0.06 μM respectively) to free DOX towards MCF-7 cells. However, the corresponding IC50 values toward MCF-7/ADR cells (9.5 and 3.4 μM for GDD and BPGDD, respectively) were 26- and 67-fold lower than that for free DOX, suggesting the GNR based nanomedicine formulation greatly improved cytotoxicity of DOX toward MDR cells. The greatly increased cytotoxicity here was fully consistent with the significantly increased cellular uptake and reduced drug efflux of the BPGDD as observed in Fig.6.

Table 2. The IC50 and resistance reversion index (RRI) of Free DOX, GDD and BPGDD against MCF MCF-7/ADR cells.

Treatment	IC50 (μM)		RRI
	MCF-7	MCF-7/ADR	
Free DOX	0.21	251	–
GDD	0.17	9.5	26
BPGDD	0.06	3.7	67

458 Resistance reversion index (RRI), ratio of IC50 of free DOX solution to nanomedicincs,
459 RRI=IC50(free DOX)/IC50(GDD or BPGDD)
460
461 The cytotoxicity of free DOX, Biotin-PEG-GNR and BPGDD (contain 2 μM DOX) towards MCF-7/ADR cells
462 induced by photothermal heating was assessed by MTT assay. Fig. 8C showed that NIR irradiation of free
463 DOX treated MCF-7/ADR cells showed negligible effect on cell viability. Similarly, NIR irradiation of Biotin-
464 PEG-GNR treated cells did not produce any significant increase of inhibition rate either, suggesting that the
465 photothermal heating alone generated by the NIR radiation here was below cell killing threshold. Fig. 8E
466 compared the inhibition rates of BPGDD treated MCF-7/ADR cells with different NIR radiation conditions.
467 Applying 2.5 w/cm^2 NIR irradiation for up to 30 min produced negligible changes of the BPGDD cytotoxicity.
468 Increasing the power density to 5 w/cm^2 produced a radiation-time dependent significantly increased inhibition
469 rate towards MCF-7/ADR cells, where 81% inhibition rate was obtained with 30 min radiation, which is more
470 than twice that without NIR irradiation. Further increasing the laser power density to 7.5 w/cm^2 produced a
471 more rapid result, where a 5 min radiation led to 78% cell inhibition rate. This observation was well
472 corresponded with the findings from the experiment of temperature increase of BPGDD solution in response
473 to NIR irradiation at different power densities. 5 min radiation at 7.5 w/cm^2 was able to produce a greater
474 temperature increase than that at 5.0 w/cm^2 for 30 min (see Fig. 5F). The impressive cell inhibition rate with
475 NIR laser radiation was mainly due to NIR radiation triggered efficient DOX release and trafficking into the cell
476 nucleus, leading to the greatly enhanced cell-killing activity [65].
477
478 *3.6. Apoptosis studies*

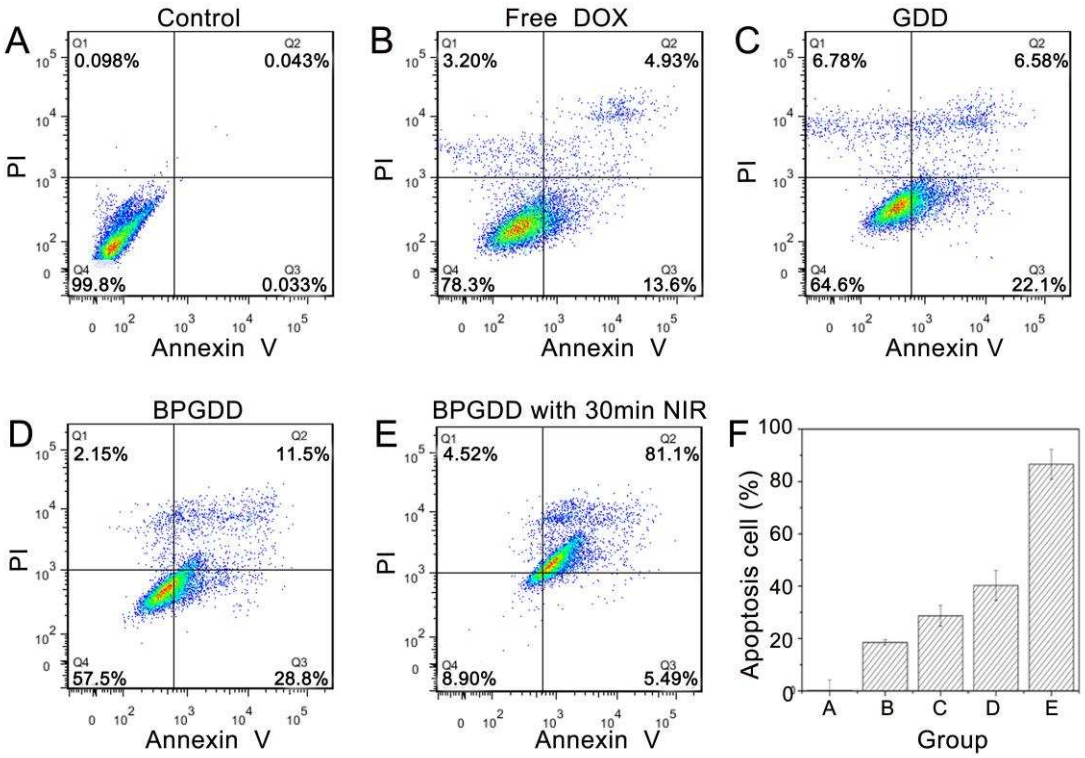

Fig. 9. Measurement of apoptosis of MCF-7/ADR cells alone (A) and the cells treated with free DOX (B), GDD (C), BPGDD (D), and BPGDD with NIR irradiation (5 w/cm^2) for 30 min (E). The cells were treated with free DOX (2 μM) or different GNR-based nanomedicines (containing 2 μM DOX and GNR 5.82μg/mL) for 4 h at 37°C, irradiated for 30 min at 5 W/cm^2 (only for E), and further incubated in fresh media for 48 h. (F) Histogram showing the percentages of apoptotic cells in (A-E). Data are presented as mean ± SD (n=3).

Annexin-V/propidium iodide (PI) double staining was performed to determine cell apoptosis. As shown in Fig.9, the percentage of apoptotic cells (sum of late apoptosis percentage (Q2) and early apoptosis percentage (Q3)) was 18.5% (Q2 and Q3, 4.93% and 13.6%) when MCF-7/ADR cells were treated with free DOX. It was increased to 28.7% (Q2 and Q3, 6.58% and 22.1%) and 40.3% (Q2 and Q3, 11.5% and 28.8%) when cells were treated with GDD and BPGDD, respectively, consistent to the enhanced drug delivery and controlled release of DOX into the cell interior by the GNR-DNA carriers as observed in cell uptake studies. Upon treatment with the BPGDD for 4 h and then exposure to NIR irradiation at 5 W/cm^2 for 30 min, the percentage of apoptotic cells reached 86.6%, further confirming the previous results that the NIR irradiation significantly increased cell apoptosis rate [66,67].

4. Conclusions

In conclusion, we have developed a pH-responsive DNA-GNR based nanomedicine that offers convenient loading of a model clinical chemotherapeutic drug (DOX) in native format via intercalation while allows for pH- and NIR-light dual-stimuli-trigged efficient drug release. Biotin-PEG functional of the GNR nanomedicine has

greatly increased its cell uptake and reduced the drug efflux ability by multidrug resistance MCF-7/ADR cells. Moreover, NIR-laser radiation has found to not only increase the DOX release, but also facilitate the drug's nucleus accumulation. As a result, this multifunctional nanomedicine substantially enhanced the cytotoxicity (by 67 fold) of free DOX towards multidrug resistance MCF-7/ADR cells. Combining abilities of targeted delivery, controlled dual-stimuli-responsive release and photothermal therapy, this DNA-GNR based multifunctional nanomedicine appears to be a highly promising, effective anticancer nanomedicine for treatment of multidrug resistant cancer at cellular or even in vivo levels.

Acknowledgements

This work is supported by xxxxxxxxxxxxxxxxxxxxxxxxxxx and the European Union FP7 Marie Curie fellowship (grant no. PIIF-GA-2012-331281). R.C. also thanks Imperial College London for funding support.

Appendix A. Supplementary data

Supplementary data to this article can be found online at XXX.

References

[1]A. Jemal, F. Bray, M.M. Center, J. Ferlay, E. Ward, D. Forman, Global cancer statistics, CA–Cancer. J. Clin. 61 (2011) 69-90.

[2]B.A. Chabner, T.G. Roberts, Timeline: Chemotherapy and the war on cancer, Nat. Rev. Cancer 5 (2005) 65-72.

[3]J.H. Gerlach, N. Kartner, D.R. Bell, V. Ling, Multidrug resistance, Cancer Surv. 5 (1986) 25-46.

[4]J.I. Fletcher, M. Haber, M.J. Henderson, M.D. Norris, ABC transporters in cancer: more than just drug efflux pumps, Nat. Rev. Cancer 10 (2010) 147-156.

[5]J.P. Gillet, M.M. Gottesman, Mechanisms of MultiDrug Resistance in Cancer, Methods Mol. Biol. 596 (2009) 47-76.

[6]X. Dong, R.J. Mumper, Nanomedicinal strategies to treat multidrug-resistant tumors: current progress, Nanomedicine 5 (2010) 597-615.

[7]S. Nobili, I. Landini, T. Mazzei, E. Mini, Overcoming tumor multidrug resistance using drugs able to evade P-glycoprotein or to exploit its expression, Med. Res. Rev. 32 (2012) 1220-1262.

[8]G.D. Leonard, T. Fojo, S.E. Bate, The role of ABC transporters in clinical practice, Oncologist 8 (2003) 411-424.

[9]G. Szakacs, J.K. Paterson, J.A. Ludwig, C. Booth-Genthe, M.M. Gottesman, Targeting multidrug resistance in cancer, Nat. Rev. Drug Discov. 5 (2006) 219-234.

[10]M.M. Gottesman, I. Pastan, Biochemistry of multidrug resistance mediated by the multidrug transporter, Annu. Rev. Biochem. 62 (1993) 385-427.

[11]T.W. Loo, D.M. Clarke, Recent progress in understanding the mechanism of P-glycoprotein mediated drug efflux, J. Membr. Biol. 206 (2005) 173-185.
[12]M.M. Gottesman, T. Fojo, S.E. Bate, Multidrug resistance in cancer: role of ATP-dependent transporters, Nat. Rev. Cancer 2 (2002) 48-58.
[13]K.T. Oh, H.J. Baik, A.H. Lee, Y.T. Oh, Y.S. Youn, E.S. Lee, The reversal of drug-resistance in tumors using a drug-carrying nanoparticular system, Int. J. Mol. Sci. 10 (2009) 3776-3792.
[14]H. Onyuksel, E. Jeon, I. Rubinstein, Nanomicellar paclitaxel increases cytotoxicity of multidrug resistant breast cancer cells, Cancer Lett. 274 (2009) 327-330.
[15]S.M. Lee, H.J. Kim, S.Y. Kim, M.K. Kwon, S. Kim, A. Cho, M. Yun, J.S. Shin, K.H. Yoo Drug-loaded gold plasmonic nanoparticles for treatment of multidrug resistance in cancer, Biomaterials 35 (2014) 2272-2282.
[16]F. Wang, Y.C. Wang, S. Dou, M.H. Xiong, T.M. Sun, J.Wang, Doxorubicin-Tethered Responsive Gold Nanoparticles Facilitate Intracellular Drug Delivery for Overcoming Multidrug Resistance in Cancer Cells, ACS nano. 5 (2011) 3679-3692.
[17]A. Albanese, P.S. Tang, W.C.W. Chan, The Effect of Nanoparticle Size, Shape and Surface Chemistry on Biological Systems, Annu. Rev. Biomed. Eng. 14 (2012) 1-16.
[18]R.K. Jain, T. Stylianopoulos, Delivering nanomedicine to solid tumor, Nat. Rev. Clin. Oncol. 7 (2010) 653-664.
[19]Y.H. Bae, K. Park, Targeted drug delivery to tumors: myths, reality and possibility, J. Control. Release 153 (2011) 198-205.
[20]M.K. Yu, J. Park, S. Jon, Targeting strategies for multifunctional nanoparticles in cancer imaging and therpy, Theranostics 2 (2012) 3-44.
[21]P. Huang, C. Xu, J. Lin, C. Wang, X.S. Wang, C.L. Zhang, X.J. Zhou, S.W. Guo, D.X. Cui, Folic acid-conjugated grapheme oxide loaded with photosensitizers for targeting photodynamic therapy, Theranostics 1 (2011) 240-250.
[22]M. Ferrari, Cancer nanotechnology: opportunities and challenges, Nat. Rev. Cancer. 5 (2005) 161-171.
[23]A. Liopo, A. Conjusteau, D. Tsyboulski, B. Ermolinsky, A. Kazansky, A. Oraevsky, Biocompatible gold nanorod conjugates for preclinical biomedical research, J. Nanomed. Nanotechnol. (2012) S2:001.
[24]A.V. Liopo, A. Conjusteau, M. Konopleva, M. Andreeff, A.A. Oraevsky, Laser nanothermolysis of human leukemia cells using functionalized plasmonic nanoparticles, Nano. Biomed. Eng. 4 (2012) 66-75.
[25]C.S. Rejiya, K. Jatish, V. Raji, M. Vibin, A. Annie, Laser immunotherapy with gold nanorods causes selective killing of tumour cells, Pharmacol. Res. 65 (2012) 261-269.
[26]J. Wang, K. Sefah, M.B. Altman, T. Chen, M.X. You, Z.L. Zhao, C.Z. Huang, W.H. Tan, Aptamer-conjugated nanorods for targeted photothermal therapy of prostate cancer stem cells, Chem. Asian J. 8 (2013) 2417-2422.
[27]X.J. Yang, X. Liu, Z. Liu, F. Pu, J.S. Ren, X.G. Qu, Near-infrared light-triggered,targeted drug delivery to cancer cells by aptamer gated nanovehicles, Adv. Mater. 24 (2012) 2890-2895.
[28]H. Jin, P.H. Yang, J.Y. Cai, J.H. Wang, M. Liu, Photothermal effects of folate-conjugated Au nanorods on

577 HepG2 cells, Appl. Microbiol. Biotechnol. 94 (2012) 1199-1208.
578 [29]F.H. Wang, Y.Y. Shen, W.J. Zhang, M. Li,Y. Wang, D.J. Zhou, S.R. Guo, Efficient, dual-stimuli responsive
579 cytosolic gene delivery using a RGD modified disulfide-linked polyethylenimine functionalized gold
580 nanorod, J. Control. Release. 196 (2014) 37–51.
581 [30]Y.L. Xiao, H. Hong, V.Z. Matson, A. Javadi, W.J. Xu, Y.N. Yang, Y. Zhang, J.W. Engle, R.J. Nickle, W.B.
582 Cai, D.A. Steeber, S.Q. Gong, Gold nanorods conjugated with doxorubicin and cRGD for combined
583 anticancer drug delivery and PET imaging, Theranostics 2 (2012) 757-768.
584 [31]L. Vigderman, B.P. Khanal, E.R. Zubarev, Functional Gold Nanorods: Synthesis, Self-Assembly, and
585 Sensing Applications, Adv. Mater. 24 (2012) 4811–4841.
586 [32]X. Wang, M.Q. Shao, S. Zhang, X.L. Liu, Biomedical applications of gold nanorod-based multifunctional
587 nano-carriers, J. Nanopart. Res. 15 (2013) 1892.
588 [33]Z.J. Zhang, J. Wang, C.Y. Chen, Gold nanorods based platforms for light-mediated theranostics,
589 Theranostics 3 (2013) 223-238.
590 [34]E.B. Dickerson, Er.C. Dreaden, X.H. Huang, I.H. El-Sayed, H.H. Chu, S. Pushpanketh, J.F. McDonald,
591 M.A. El-Sayed, Gold nanorod assisted near-infrared plasmonic photothermal therapy(PPTT) of squamous
592 cell carcinoma in mice, Cancer Lett. 269 (2008) 57-66.
593 [35]W.I. Choi, J.Y. Kim, C. Kang, C.C. Byeon, Y.H. Kim, G. Tae, Tumor regression in vivo by photothermal
594 therapy based on gold-nanorod-loaded,functional nanocarriers, ACS Nano. 5 (2011) 1995-2003.
595 [36]G.V. Maltzah, J.H. Park, A. Agrawal, N.K. Bandaru, S.K. Das, M.J. Sailor, S.N. Bhatia, Computationally
596 guided photothermal tumor therapy using long-circulating gold nanorod antennas, Cancer Res. 69 (2009)
597 3892-3900.
598 [37]B.K. Wang, J.H. Wang, Q. Liu, H. Huang, M. Chen, K.Y. Li, C.Z. Li, X.F. Yu, P.K. Chu, Rose-bengal-
599 conjugated gold nanorods for in vivo photodynamic and photothermal oral cancer therapies, Biomaterials
600 35 (2014) 1954-1966.
601 [38]E. Lee, Y. Hong, J. Choi, S. Haam, J.S. Suh, Y.M. Huh, J. Yang, Highly selective CD44-specific gold
602 nanorods for photothermal ablation of tumorigenic subpopulations generated in MCF7 mammospheres,
603 Nanotechnology 23 (2012) 465101.
604 [39]J. Choi, J. Yang, D. Bang, J. Park, J.S. Suh, Y.M. Huh, S. Haam, Targetable gold nanorods for epithelial
605 cancer therapy guided by near-IR absorption imaging, Small 8 (2012) 746-753.
606 [40]K.C.L. Black, J. Yi, J.G. Rivera, D.C. Zelasko-Leon, P.B. Messersmith, Polydopamine-enabled surface
607 functionalization of gold nanorods for cancer cell-targeted imaging and photothermal therapy,
608 Nanomedicine 8 (2013) 17-28.
609 [41]L.E. Gerweck, K. Seetharaman, Cellular pH Gradient in Tumor versus Normal Tissue: Potential
610 Exploitation for the Treatment of Cancer, Cancer Res. 56 (1996) 1194.
611 [42]R.J. Lee, S. Wang, P.S. Low, Measurement of endosome pH following folate receptor-mediated
612 endocytosis, Biochem. Biophys. Acta 1312 (1996) 237-242.
613 [43]K. Gehring, J.L. Leroy, M. Gueron, A tetrameric DNA structure with protonated cytosine-cytosine base
614 pairs, Nature 363 (1993) 561-565.

615 [44]X. Hou, W. Guo, F. Xia, F.Q. Nie, H. Dong, Y. Tian, L.P. Wen, L. Wang, Li.X. Cao, Y. Yang, J.M. Xue, Y.L.
616 Song, Y.G. Wang, D.S. Liu, L. Jiang, A Biomimetic Potassium Responsive Nanochannel: G-Quadruplex
617 DNA Conformational Switching in a Synthetic Nanopore, J. Am. Chem. Soc. 131 (2009) 7800–7805.
618 [45]J. Choi, T. Majima, Reversible Conformational Switching of i-Motif DNA Studied by Fluorescence
619 Spectroscopy, Photochem. Photobiol. 89 (2013) 513–522.
620 [46]W.X. Wang, Y. Yang, E.J. Cheng, M.C. Zhao, H.F. Meng, D.S. Liu, D.J. Zhou, A pH-driven, reconfigurable
621 DNA nanotriangle, Chem. Commun. 7 (2009) 824–826.
622 [47]D.S. Liu, A. Bruckbauer, C. Abell, S. Balasubramanian, D.J. Kang, D. Klenerman, D.J. Zhou, A Reversible
623 pH-Driven DNA Nanoswitch Array, J. Am. Chem. Soc. 128 (2006) 2067-2071.
624 [48]W.M. Shu, D.S. Liu, M. Watari, C.K. Riener, T. Strunz, M.E. Welland, S. Balasubramanian, R.A. McKendry,
625 DNA Molecular Motor Driven Micromechanical Cantilever Arrays, J. Am. Chem. Soc. 127 (2005) 17054-
626 17060.
627 [49]P.F. Zhan, J.Y. Wang, Z.G. Wang, B.Q. Ding, Engineering the pH-Responsive Catalytic Behavior of AuNPs
628 by DNA, Small 10 (2014) 399–406.
629 [50]W. Li, J.S. Wang, J.S. Ren, X.G. Qu, Near-Infrared- and pH-Responsive System for Reversible Cell
630 Adhesion using Graphene/Gold Nanorods Functionalized with i-Motif DNA, Angew. Chem. Int. Ed. 52
631 (2013) 6726 –6730.
632 [51]D. Zhao, Z.L. Zhang, Y.Q. Wen, X.J. Zhang, Y.L. Song, Reversible gold nanorod assembly triggered by
633 pH-responsive DNA nanomachine, Appl. Phys. Lett. 102 (2013) 123101.
634 [52]T. Liedl, F.C. Simme, Switching the Conformation of a DNA Molecule with a Chemical Oscillator, Nano
635 Lett. 5 (2005) 1894-1898.
636 [53]L. Han, R.Q. Huang, J.F. Li, S.H. Liu, S.X. Huang, C. Jiang, Plasmid pORF-hTRAIL and doxorubicin co-
637 delivery targeting to tumor using peptide-conjugated polyamidoamine dendrimer. Biomaterials. 32 (2011)
638 1242-1252.
639 [54]L. Song, V.H.B. Ho, C. Chen, Z.Q. Yang, D.S. Liu, Ro.J. Chen, D.J. Zhou, Efficient, pH-Triggered Drug
640 Delivery Using a pH-Responsive DNA-Conjugated Gold Nanoparticle, Adv. Healthcare Mater. 2 (2013)
641 275–280.
642 [55]L. Song, Y. Guo, D. Roebuck, C. Chen, M. Yang, Z.Q. Yang, S. Sreedharan, C. Glover, J.A. Thomas, D.S.
643 Liu, S.R. Guo, R.J. Chen, D.J. Zhou, Terminal PEGylated DNA−Gold Nanoparticle Conjugates Offering
644 High Resistance to Nuclease Degradation and Efficient Intracellular Delivery of DNA Binding Agents, ACS
645 Appl. Mater. Interfaces 7 (2015) 18707-18716.
646 [56]B. Nikoobakht, M.A. El-Sayed, Preparation and growth mechanism of gold nanorods (NRs) using seed-
647 mediated growth method, Chem. Mater. 15 (2003) 1957–1962.
648 [57]X.C. Ye, L.H. Jin, H. Caglayan, J. Chen, G.Z. Xing, C. Zheng, V. Doan-Nguyen, Y.J. Kang, Na. Engheta,
649 C.R. Kagan, C.B. Murray, Improved size-tunable synthesis of monodisperse gold nanorods through the
650 use of aromatic additives, ACS Nano. 6 (2012) 2804–2817.
651 [58]Y. Wang, F.H. Wang, Y. Guo, R.J. Chen, Y.Y. Shen, A.J. Guo, J.Y. Liu, X. Zhang, D.J. Zhou, S.R. Guo,
652 Controlled synthesis of monodisperse gold nanorods with different aspect ratios in the presence of

aromatic additives. J. Nanopart. Res. 16 (2014) 2806.
[59]A. Wijaya, K. Hamad-Schifferli, Ligand customization and DNA functionalization of gold nanorods via round-trip phase transfer ligand exchange, Langmuir 24 (2008) 9966–9969.
[60]S.K. Srivastava, M.J. Modak, Rose bengal mediated inhibition of DNA polymerases: mechanism of inhibition of avian myeloblastosis virus reverse transcriptase under photooxidative conditions, Biochemistry 22 (1983) 2283-2288.
[61]G.F. Du, C.Z. Li, H.Z. Chen, X. Chen, Q. Xiao, Z.G. Cao, S.H. Shang, X. Cai, Rose bengal staining in detection of oral precancerous and malignant lesions with colorimetric evaluation: a pilot study, Int. J. Cancer 120 (2007) 1958-1963.
[62]Y.C. Wang, K.C.L. Black, H. Luehmann, W.Y. Li, Y. Zhang, X. Cai, D.H. Wan, S.Y. Liu, M. Li, P. Kim, Z.Y. Li, L.V. Wang, Y.J. Liu, Y.N. Xia, Comparison Study of Gold Nanohexapods, Nanorods, and Nanocages for Photothermal Cancer Treatment, ACS Nano. 7 (2013) 2068-2077.
[63]S. Yamashita, H. Fukushima, Y. Akiyama, Y. Niidome, T. Mori, Y. Katayama, T. Niidome, Controlled-release system of single-stranded DNA triggered by the photothermal effect of gold nanorods and its in vivo application, Bioorg. Med. Chem. 19 (2011) 2130–2135.
[64]M.F. Tsai, S.H.G. Chang, F.Y. Cheng, V. Shanmugam, Y.S. Cheng, C.H. Su, C.S. Yeh, Au Nanorod Design as Light-Absorber in the First and Second Biological Near-Infrared Windows for in Vivo Photothermal Therapy, ACS Nano. 7 (2013) 5330-5342.
[65]M. Chang, C.S. Yang, D.M. Huang, Aptamer-Conjugated DNA Icosahedral Nanoparticles As a Carrier of Doxorubicin for Cancer Therapy, ACS Nano. 5 (2011) 6156-6163
[66]X.H. Huang, I.H. El-Sayed, W. Qian, M.A. El-Sayed, Cancer Cell Imaging and Photothermal Therapy in the Near-Infrared Region by Using Gold Nanorods, J. Am. Chem. Soc. 128 (2006) 2115-2120.
[67]S.X. Huang, K. Shao, Y. Liu, Y.Y. Kuang, J.F. Li, S. An, Y.B. Guo, Ha.J. Ma, C. Jiang, Tumor-Targeting and Microenvironment-Responsive Smart Nanoparticles for Combination Therapy of Antiangiogenesis and Apoptosis, ACS Nano. 7 (2013) 2860-2871.

Figure captions:

Fig. 1. BPGDD is effectively taken up by cancer cell via binding to its over-expressed biotin receptors and entry into intracellular endosomes. The gradual acidification of the intracellular compartments following the natural endosomal maturation/trafficking pathways lead to i-motif formation and trigger DOX release. Alternatively, DOX release can also be triggered by application of a NIR radiation to locally heats up the GNR carrier.

Fig.2. (A) Principle of pH-triggered drug delivery: DOX is intercalated stably within the M1/MC2 duplex at normal physiological pH 7.4, and when pH decreases to ~5.0, M1 forms a four-stranded i-motif structure and the duplex of dsDNA dissociates and DOX is released. (B) Fluorescence spectra of DOX (20μM) with increasing the dsDNA:DOX molar ratio at pH 7.4.

Fig.3. Schematic route to preparation of (A) HS-PEG and HS-PEG-Biotin, (B) BPGDD multi-functional nanomedicine.

Fig. 4. Characterization of GNR-based systems. (A) UV–Vis–NIR absorption spectra and (B) Zeta potential of of GNR-CTAB, GNR-MUDA, GNR-PEG and BPGDD. (C) A typical TEM image of BPGDD complexes.(D) Dependence of DOX fluorescence intensity as a function of pH for the dsDNA/DOX and BPGDD systems respectively.

Fig. 5. In vitro DOX release profiles from BPGDD nano-complexes. (A) Fluorescence spectra of the time-dependent release of DOX at pH 7.4. (B) Fluorescence spectra of the time-dependent release of DOX at pH 5.0. (C) Time-dependent cumulative release of DOX at different pH values. (D) Fluorescence spectra of free DOX before and after NIR irradiation. (E) Time-dependent cumulative DOX release at different NIR radiation power densities (808 nm, 1, 2.5, 5, 7.5 and 10 W/cm^2) at pH 5.0. (F) Time-dependent change of the temperature of BPGDD solution in response to NIR irradiation at different power densities. (contain 2 μM DOX and GNR 5.82μg/mL). (G)Schematic showing that pH-triggered release alone is less effective than pH- and NIR-light dual-stimuli-triggered DOX release. Data are presented as mean ± SD (n = 3).

Fig. 6. Time-dependent cellular uptake of DOX by MCF-7 (A) and MCF-7/ADR (B) cells after incubation with free DOX, GNR-DNA/DOX(GDD) and BPGDD (contain 0.25 μM DOX), respectively. Time-dependent efflux of DOX from MCF-7 (C) and MCF-7/ADR (D) cells during the further incubation period (contain 2 μM DOX). (E) Mean DOX fluorescence intensity of MCF-7/ADR cells after incubation with BPGDD (contain 2 μM DOX and GNR 5.82μg/mL) followed by 0, 10 and 30 min of NIR irritation (808 nm, 5 w/cm^2) and 1-4 h further incubation. Data are presented as mean ± SD (n = 3).

Fig. 7. (A) Confocal fluorescence images showed the intracellular distribution of DOX in MCF-7/ADR cells after treatment with free DOX, GDD, and BPGDD (contain 2 μM DOX and GNR 5.82μg/mL) respectively for 2 or 4 h. (B)The histogram of the nuclei blue-stained with Hoechst 33342 and red-stained with DOX in the MCF-7/ADR cells treated with the BPGDD for 4 h, irradiated with NIR for 30 min or not..

Fig. 8. The inhibition rate of MCF-7 (A) and MCF-7/ADR (B) cells after incubation with free DOX, GDD and BPGDD for 48 h at 37°C as measured by MTT assay. And the inhibition rate of MCF-7/ADR cells after 4 h incubation with free DOX (C), Biotin-PEG-GNR (D), BPGDD (E) (containing 2 μM DOX and GNR 5.82μg/mL), followed by different NIR laser radiation conditions and further 48 h incubation with fresh media. Data are presented as mean ± SD (n = 3).

Fig. 9. Measurement of apoptosis of MCF-7/ADR cells alone (A) and the cells treated with free DOX (B), GDD (C), BPGDD (D), and BPGDD with NIR irradiation (5 w/cm^2) for 30 min (E). The cells were treated with free DOX (2 μM) or different GNR-based nanomedicines (containing 2 μM DOX and GNR 5.82μg/mL) for 4 h at 37°C, irradiated for 30 min at 5 W/cm^2 (only for E), and further incubated in fresh media for 48 h. (F) Histogram showing the percentages of apoptotic cells in (A-E). Data are presented as mean ± SD (n=3).